Journal of Power Sources 196 (2011) 8632–8637

Contents lists available at ScienceDirect

Journal of Power Sources

journal homepage: www.elsevier.com/locate/jpowsour

Study of the surface modification of $LiNi_{1/3}Co_{1/3}Mn_{1/3}O_2$ cathode material for lithium ion battery

A.M.A. Hashem[a], A.E. Abdel-Ghany[a], A.E. Eid[a], J. Trottier[b], K. Zaghib[b,*], A. Mauger[c], C.M. Julien[d]

[a] National Research Centre, Inorganic Chemistry Department, Behoes St., Dokki, Cairo, Egypt
[b] Hydro-Québec Research Institute (IREQ), 1800 Lionel Boulet, Québec, Canada J3X 1S1
[c] Université Pierre et Marie Curie-Paris-6, IMPMC, 4 place Jussieu, 75252 Paris, France
[d] Université Pierre et Marie Curie-Paris-6, PECSA, UMR 7195, 4 place Jussieu, 75252 Paris, France

ARTICLE INFO

Article history:
Received 19 May 2011
Received in revised form 8 June 2011
Accepted 9 June 2011
Available online 13 July 2011

Keywords:
$LiNi_{1/3}Co_{1/3}Mn_{1/3}O_2$
Surface analysis: Raman scattering
Li-ion batteries

ABSTRACT

The surface of $LiNi_{1/3}Co_{1/3}Mn_{1/3}O_2$ (LNMCO) particles has been studied for material synthesized at 900 °C by a two-step process from a mixture of $LiOH{\cdot}H_2O$ and metal oxalate [$(Ni_{1/3}Co_{1/3}Mn_{1/3})C_2O_4$] obtained by co-precipitation. Samples have been characterized by X-ray diffraction (XRD), high-resolution transmission electron microscope (HRTEM), Raman scattering (RS) spectroscopy, and magnetic measurements. We have investigated the effect of the heat treatment of particles at 600 °C with organic substances such as sucrose and starch. HRTEM images and RS spectra indicate that the surface of particles has been modified. The annealing does not lead to any carbon coating but it leads to the crystallization of the thin disordered layer on the surface of $LiNi_{1/3}Co_{1/3}Mn_{1/3}O_2$. The beneficial effect has been tested on the electrochemical properties of the $LiNi_{1/3}Co_{1/3}Mn_{1/3}O_2$ cathode materials. The capacity at 10C-rate is enhanced by 20% for post-treated LNMCO particles at 600 °C for half-an-hour.

1. Introduction

Lithium ion batteries (LIB) have been widely used to power portable electronic equipments, and have long been considered as possible power sources for electric or hybrid vehicles. Cathode materials play an important role on determining performances of lithium ion batteries. $LiCoO_2$ (LCO) is the most popular cathode material so far used in lithium-ion batteries since its first introduction by Sony in 1990 [1]

More recently, Ohzuku and Makimura have suggested the layered transition-metal oxide $LiNi_{1/3}Co_{1/3}Mn_{1/3}O_2$ (LNMCO) with rhombohedral structure as an alternative to LCO [2]. This material has attracted significant interest because the combination of nickel, manganese and cobalt can provide advantages such as higher reversible capacity, lower material cost, and milder thermal stability. Currently, $LiNi_{1/3}Co_{1/3}Mn_{1/3}O_2$ is considered to be one of the best candidates for the cathode material in lithium ion batteries to replace the presently popular $LiCoO_2$ [3] because of the absence of the monoclinic distortion at the half-delithiated charge state [4]. However, the preparation of high performance $LiNi_{1/3}Co_{1/3}Mn_{1/3}O_2$ is not an easy task; a suitable preparation method must be selected to obtain phase-pure final products.

The preparation of the $LiNi_{1/3}Co_{1/3}Mn_{1/3}O_2$ solid solution with excellent electrochemical performance is challenging. Compared with the solid-state reaction method, co-precipitation method is an easier route to produce phase-pure $LiNi_{1/3}Co_{1/3}Mn_{1/3}O_2$ [5]. The hydroxide co-precipitation method has been used as a major preparation technique to get homogeneous $LiNiO_2$–$LiMnO_2$–$LiCoO_2$ solid solution [3,6–11]. Actually, it is one of the powerful synthesis methods because precipitated transition-metal hydroxide are oxidized in the aqueous solution at the molecular level; that is the reason why we have adopted it in this work.

Despite the advantage of using LNMCO in electrochemical cells, the delivered capacities have shown a fading when high-rate current density is applied. Aurbach et al. [12] have suggested that the capacity retention of a cathode active material is strongly dependent on the surface chemistry of the particles of the insertion material, which are always covered by surface films limiting the Li-ion migration and their charge transfer across the active interface. Addition of substituting element or surface modification of LCO and LNMCO has shown improvement of their performance during cycling at high rate [13–19]. Many research works confirm that such a modification of the surface of the particles is greatly beneficial, because side reactions are avoided on the surface. Among the most popular techniques reported so far, the deposit of a thin layer of metal oxides on powders of LCO results in better stability and safety of this material. For example, Chen and Dahn have shown the effectiveness of ZrO_2 coating for improving the capacity retention of LCO during the high potential cycling [20].

* Corresponding author. Tel.: +1 450 652 8019; fax: +1 450652 8424.
E-mail address: zaghib.karim@ireq.ca (K. Zaghib).

0378-7753/$ – see front matter © 2011 Elsevier B.V. All rights reserved.
doi:10.1016/j.jpowsour.2011.06.039

Similar efforts have recently made for $LiNi_{1/3}Co_{1/3}Mn_{1/3}O_2$ by covering the particles with several substances such as $LiAlO_2$ [21], Al_2O_3 [22] and carbon [23]. The carbon coating that appears successful for $LiFePO_4$ also seems efficient to improve the cycle life of Li-ion batteries with LNMCO [23] and LCO as well [24]. However, many authors did not report on the chemistry of the deposit when it exists, in which case the lack of surface analysis makes questionable the nature of the passivation layer.

In this study, we selected an oxalate co-precipitation method using oxalic acid for the synthesis of the $LiNi_{1/3}Co_{1/3}Mn_{1/3}O_2$ material. The homogeneous solid solution containing mixture of Ni, Co and Mn ions could be readily obtained by method. The surface layer of the LNMCO particles has been modified by mixing them with an organic substance such as sucrose and starch followed by an annealing process at moderate temperature ($T > 700\,^{\circ}C$). Samples were characterized by X-ray diffraction (XRD), high-resolution transmission electron microscope (HRTEM), Raman scattering (RS) spectroscopy and SQUID magnetometry. The beneficial effect was tested on the electrochemical properties of the $LiNi_{1/3}Co_{1/3}Mn_{1/3}O_2$ cathode materials.

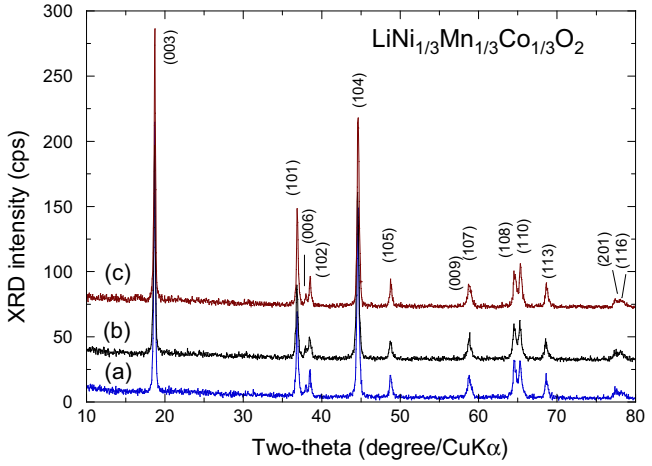

Fig. 1. XRD patterns of LNMCO materials synthesized by co-precipitation method: (a) as-grown, (b) heat treated with sucrose and (c) heat treated with starch. All the Bragg peaks are indexed in the hexagonal sitting of the *R-3m* symmetry.

2. Experimental

2.1. Synthesis

We have chosen the wet-chemical synthesis, i.e. co-precipitation method, to reduce the size of the particles with respect to the solid-state reaction (see [23] and references therein). Nickel, cobalt and manganese oxalate ($(Ni_{1/3}Co_{1/3}Mn_{1/3})C_2O_4$(precursor was synthesized by a co-precipitation method using aqueous solution of $Ni(NO_3)_2{\cdot}6H_2O$, $Co(NO_3)_2{\cdot}6H_2O$ and $Mn(NO_3)_2{\cdot}4H_2O$ (cationic ratio of Ni/Co/Mn = 1:1:1), in which 100 mL 1M oxalic acid was drowsily added by stirring until the complete precipitation of oxalate precursor. The product was filtered, and dried at 100 °C for 12 h. Then, a stoichiometric amount of lithium hydroxide was mixed thoroughly with the dried powder and calcined at 900 °C for 12 h in air to obtain the final $LiNi_{1/3}Co_{1/3}Mn_{1/3}O_2$ powders (named bare-LNMCO hereafter). The surface modification was made by mixing 2 g of $LiNi_{1/3}Co_{1/3}Mn_{1/3}O_2$ with 0.1 g sucrose (3 wt.%) in an agate mortar for more than 2 h. After an intimate mixing, the powders were heat treated at 600 °C for half-an-hour in air. Similar procedure was made using starch instead of sucrose as carbon source. Note the time spent at 600 °C is an important parameter because of the reaction of the carbon with oxygen in the air.

2.2. Apparatus

The crystal structure of the prepared samples was analyzed by X-ray diffractometry (XRD) using Philips X'Pert apparatus equipped with a CuK_α X-ray source ($\lambda = 1.5406$ Å). XRD measurements were collected in the 2θ range 10–80°. Raman spectra were obtained with a micro-Raman spectrophotometer (Horiba) coupled with an optical microscope. Measurements were carried out using a 633 nm He–Ne laser excitation line and recorded in steps of 1.6 cm^{-1} with an acquisition time of 30 s. A 100× microscope objective was employed to focus the laser beam and to collect the scattered light, providing a 1-μm-diameter laser spot. Care was taken against sample photodecomposition using a low excitation power 100 W cm^{-2}. The wavenumber calibration was regularly verified by using the Raman peak at 520 cm^{-1} of a silicon crystal as a reference. HRTEM images were obtained using an electronic microscope Hitachi model H-9000 working at a potential of 300 kV. For TEM analysis, the powder sample was dispersed on a 3-mm Cu-grid with a hole size of 1 mm × 2 mm. The TEM samples were ultrasonically treated in a solution of isopropyl alcohol and then deposited on silica substrate. Magnetic measurements (susceptibility and magnetization) were carried out with a fully automated SQUID magnetometer (MPMS-5S from Quantum Design) using the procedure described elsewhere [25].

The electrochemical properties of the product were tested at 25 °C in cells with metallic lithium as the negative electrode using Teflon laboratory-cell hardware and Mac-Pile system. The non-aqueous electrolyte was 1.0 mol L^{-1} $LiClO_4$ dissolved in propylene carbonate (PC). The active electrode material was deposited onto Al foil at the loading 8.8 mg cm^{-2}. Charge and discharge processes were carried out at C/12 rate in the voltage range 3.0–4.4 V vs. Li^0/Li^+.

3. Results and discussion

3.1. Structural study

The XRD patterns of the bare LNMCO and carbon treated samples are shown in Fig. 1. The diagrams reveal that all samples have a typical structure of a hexagonal α-$NaFeO_2$ type for which patterns can be indexed with the *R-3m* space group. In order to determine accurately the structure of samples, refinement by the Rietveld method of the XRD data was performed, using the model $[Li_{1-\delta}Ni_\delta]_{3b}[Li_\delta Ni_{x-\delta}Mn_yCo_{1-x-y}]_{3a}O_2$ [26]. As an example, the Rietveld fit of the XRD spectrum for the as-grown samples is shown in Fig. 2. The lattice parameters of the different samples are reported in Table 1. Several characteristics indicate the high crystallinity of the samples: (i) the narrow Bragg lines, (ii) the splitting of the (0 0 6)/(1 0 2) and (1 0 8)/(1 1 0) doublets [27] and (iii) the integrated intensity ratio of (0 0 3) and (1 0 4) peaks $I_{(003)}/I_{(104)}$ should be higher than 1.2 [28], which condition is fulfilled in our case (see Table 1). These properties also give an indication that this sample has a very small cation mixing, i.e. a very small concentration of Ni^{2+} ions in the Li(3*b*) interlayer sites [29], and suggests a homogeneous distribution of cations within the structure. In addition, the *c*/*a* value can also indicate the degree of trigonal distortion, a higher cation ordering due to this distortion being achieved when *c*/*a* value is higher than 4.899 [30]. Indeed, the concentration of Ni(3*b*) defects and then the Li^+/Ni^{2+} cation mixing deduced from the Rietveld refinement is only 2.04%. All these parameters do not change significantly upon heat treatment. The coherence length estimated from the Scherrer formula is $L = 167 \pm 8$ nm.

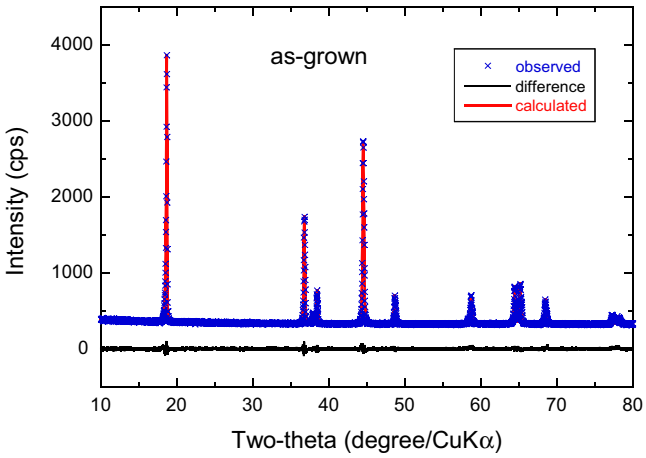

Fig. 2. Rietveld refinement patterns of the as-grown LNMCO sample. The cross marks show observed XRD intensities and the solid line represents calculated intensities. The curve at the bottom is the difference between the calculated and observed intensities on the same scale.

3.2. Study of the surface of particles

Fig. 3 displays four TEM pictures of $LiNi_{1/3}Co_{1/3}Mn_{1/3}O_2$ powders. The typical images (a–b) for as-grown LNMCO and heat treated sample, respectively, show an average particle size of 250 nm. Images (c) and (d) are the HRTEM features of LNMCO powders for as-grown and heat-treated sample with sucrose at 600 °C for 30 min in air, respectively. The powders are composed of well-dispersed monocrystallite particles, which are slightly agglomerated and show a small quantity of fragments. We observe similar features at any part of the samples, which appear to be homogeneous at a large scale with respect to the area investigated. The particle size deduced from TEM is in agreement with the coherent length of X-rays evaluated by the Scherrer formula.

Table 1
Lattice parameters of LNMCO samples.

Compound	a (Å)	c (Å)	V (Å^3)	c/a	I_{003}/I_{104}
As-grown	2.899(3)	14.285(5)	103.96(9)	4.93	1.43(1)
Sucrose	2.902(4)	14.326(5)	104.51(3)	4.94	1.44(1)
Starch	2.912(7)	14.392(4)	105.74(2)	4.94	1.44(7)

The analysis of the HRTEM images gives evidence that the surface of the particles have been modified by the calcination at 600 °C. Fig. 3c displays clearly the presence of an amorphous-like layer, typically 2.5 nm thick, that covers the LNMCO particle synthesized by co-precipitation method via oxalate route. In the HRTEM micrograph, this surface layer appears as a grayish region at the edge of the $LiNi_{1/3}Co_{1/3}Mn_{1/3}O_2$ crystallites, while the core of the primary particle is the dark region. After the heat-treatment at moderate temperature with an organic substance such as sucrose or starch, we observe the disappearance of disordered layer. It is well illustrated in Fig. 3d. Note the quality of the sample surface depends strongly of the annealing duration at 600 °C due to the reaction of the carbon with oxygen in the air. A heat treatment during half-an-hour is needed for complete crystallization of the surface layer.

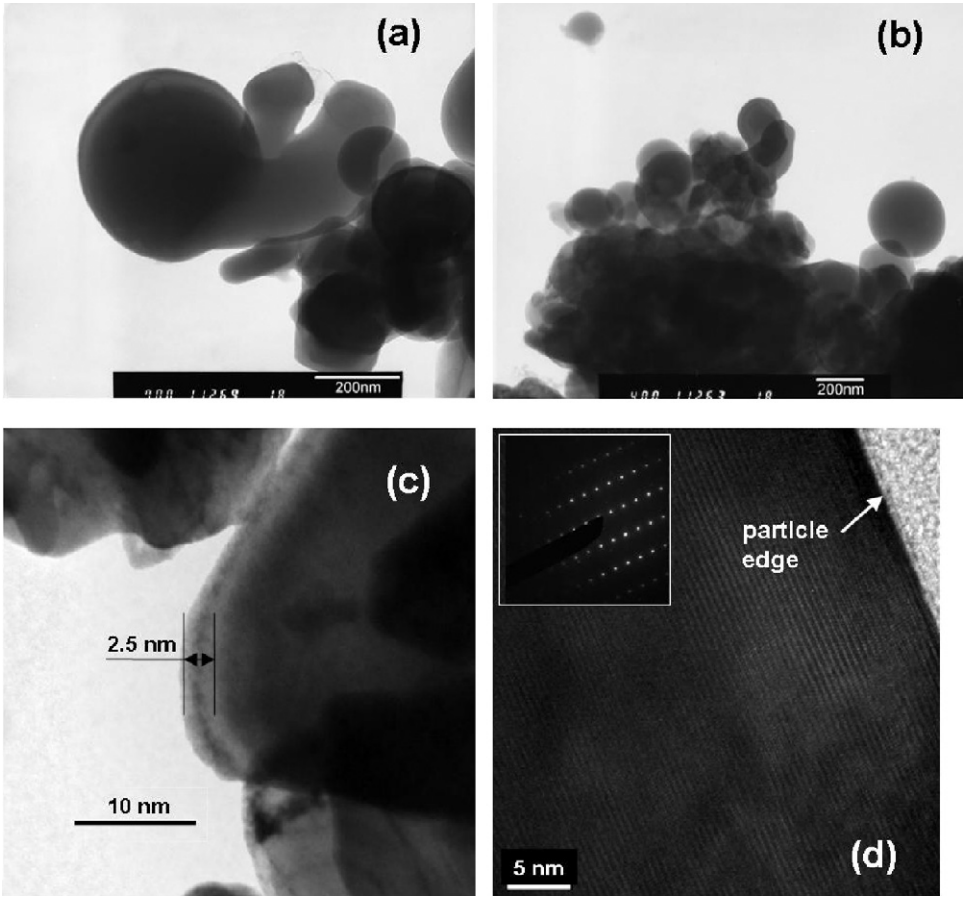

Fig. 3. (a) and (b) TEM images of LNMCO powders showing an average particle size of 250 nm. Images (c) and (d) display the HRTEM features of LNMCO powders for as-grown and heat treated sample with sucrose at 600 °C for 30 min in air, respectively.

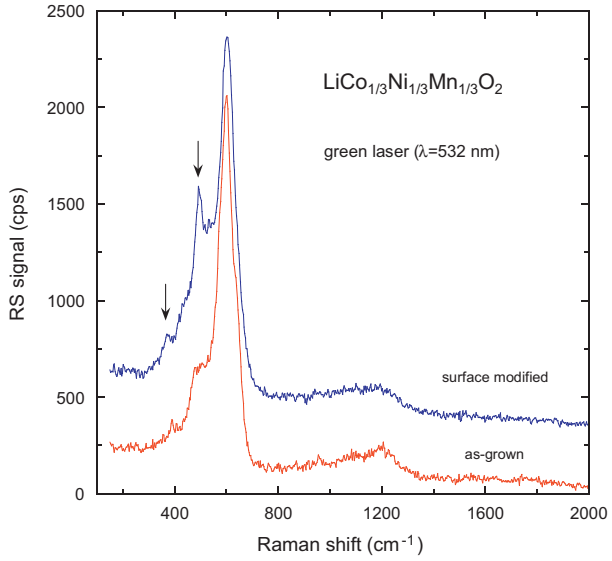

Fig. 4. Raman scattering spectra of LNMCO powders: (a) as-grown sample and (b) surface modified sample heat-treated at 600 °C for 30 min in air with sucrose. Spectra were recorded using the 633 nm excitation laser line at the 1 cm^{-1} spectral resolution. Note that Raman-active bands due to carbon are not observed.

To characterize quantitatively the surface modification, we have chosen to investigate it a Raman scattering spectroscopy that is a powerful tool for such a purpose. Raman spectroscopy is sensitive to the short-range environment of oxygen coordination around the cations in oxide lattices [31]. The frequencies and the relative intensities of the bands are sensitive to the coordination geometry and the oxidation state of the cations. In addition, this technique is considered as a useful probe for surface analysis, especially when the material is a high absorber of the visible light. In this case the penetration depth of the laser beam could be estimated from the attenuation given by the absorbing material, a value of few 10 nm is obtained for $LiNi_{1/3}Co_{1/3}Mn_{1/3}O_2$. Therefore, Raman spectroscopy is well suited to the analysis of the surface layer of particles. Fig. 4 shows the Raman spectra of the as-grown LNMCO powder (a) and surface-modified sample after heat-treatment at 600 °C for 30 min in air with sucrose (b). These data clearly evidence the Raman-active E_g and A_{1g} modes for the layered $LiNi_{1/3}Co_{1/3}Mn_{1/3}O_2$ in the D^5_{3h} spectroscopic symmetry, while none of Raman-active bands due to carbon is detected. The peaks currently called D and G expected at 1350 and 1580 cm^{-1}, respectively, [32–34] are absent.

However, we observe a strong effect on the low-frequency peaks in the spectral range 400–550 cm^{-1}, i.e. the region of the symmetric bending modes of the LNMCO material. The Raman spectrum of the as-grown sample exhibits poor-resolved peaks, corresponding to a highly disordered surface layer; the disorder is responsible for the broader density of state and shorter lifetime of the phonons evidenced in the Raman spectrum. After sugar treatment the low frequency peaks are well defined (marked by arrow), which means a recrystallization of the surface layer. This is the proof that the heat treatment at 600 °C in presence of sugar has recrystallized the surface, without formation of a carbon coating thick enough to be detected by Raman spectroscopy.

It seems that the lack of carbon coating is due to the low-temperature process, $T < 700$ °C, used in our work. In general, the carbon pyrolysis starts to be efficient at $T > 750$ °C [34]. It could be remarked that numerous workers claimed the coating of many substances such as carbon, alumina, zirconia among others, but never investigated the deposit by surface analysis methods [12–24], excepted few groups reporting elemental analysis by SIMS and XPS [15,17] and depth profile by Auger spectroscopy [14]. Of course, they demonstrated improvements in the electrochemical features of the cathode materials, which should be due to the coating rather than the reconstruction of the surface layer. Another reason for the lack of carbon coating is the small amount of carbon (3 wt.%) that has been added to the product before heating at 600 °C. These experiments have shown that the calcination at 900 °C is still too low to cure the surface disorder. Therefore the presence of sugar, in the present case, is the key element that allows for the surface crystallization during the post-annealing process at 600 °C.

It is difficult to attribute the re-crystallization of the surface layer to the carbon itself, since any carbothermal effect requires temperatures $T \geq 1000$ °C. The hydrogen contained in the sugar or the starch is a reducing agent, which plays an important role in the case of another cathode element for Li-ion batteries, $LiFePO_4$. However in this particular case, it is essentially due to a specific interaction of iron with organic compounds [35]. In the present case, the absence of coating suggests that the role played by the organic compound is not so important. The re-crystallization of the surface layer evidenced by both the HRTEM and the Raman spectroscopy experiments are then more likely attributable to a thermal effect, namely the disorder is simply cured by the calcination at 600 °C [36].

3.3. Estimation of the cation mixing

The temperature dependence of the reciprocal magnetic susceptibility $\chi_m^{-1} = H/M$ of LNMCO samples and the isothermal curves of the magnetic moment $M(H)$ carried out by the TM cations are reported in Fig. 5a and b.

Above 150 K, the linear variations of χ_m^{-1} with T can be described again by Curie–Weiss law: $\chi_m^{-1} = (T - \Theta_p)/C_p$, with Θ_p the Weiss temperature, and C_p the Curie constant related to the effective magnetic moment μ_{eff} by the relation $C_p = N\mu_{eff}^2/3k_B$, with k_B the Boltzmann constant and N the number of metal ions in one mole of product. The values of the two fitting parameters Θ_p and μ_{eff} are $\Theta_p = -72 \pm 2$ K and and $\mu_{eff} = 2.72 \pm 0.02$ μ_B for the three samples. The negative value of Θ_p is an intrinsic property due to the fact that the magnetic interactions are mainly the intra-layer superexchange interactions mediated via oxygen at 90° bonding angle, and they are dominantly antiferromagnetic [37,38]. Considering the charge distribution such as Ni^{2+}, Mn^{4+} and Co^{3+}(LS), the experimental values of μ_{eff} is close to the theoretical value of the effective magnetic moment per chemical formula in the paramagnetic regime given by

$$\mu_{theor} = 1/3(\mu^2_{Ni^{2+}} + \mu^2_{Mn^{4+}} + \mu^2_{Co^{3+}}) = 2.77\mu_B, \quad (1)$$

where $\mu_{Ni^{2+}} = 2.83\mu_B$, $\mu_{Mn^{4+}} = 3.87\mu_B$ and $\mu_{Co^{3+}} = 0$. We note that the heat treatment at 600 °C does not modify the magnetic properties of the core of LNMCO particles.

The isothermal curves of the magnetic moment $M(H)$ show a linear behaviour (Fig. 5b) with the applied magnetic field, except at very low temperature ($T < 10$ K) for which the non-linearity of $M(H)$ is due to the ferromagnetic spin freezing of the $Mn^{4+}(3a)$–$Ni^{2+}(3b)$ pair at low temperature. Thus, the magnetization of this pair is saturated and the contribution of the orbital momentum is negligible, since it is quenched by the crystal-field. This saturated effective spin gives a contribution $g\mu_B(S_{Mn} + S_{Ni}) = 2(3/2 + 1)$ $\mu_B = 5$ μ_B to the magnetization at large value of H, giving rise to the magnetization M_S measured by extrapolation of $M(H)$ from large values of H to $H = 0$ (Fig. 5b). The result for the estimation of the rate of cation mixing deduced from this magnetic analysis is in remarkable agreement with the result deduced from Rietveld refinement for all the samples investigated. In the case of the $LiNi_{1/3}Co_{1/3}Mn_{1/3}O_2$ sample synthesized by the oxalate route, we find $M_s = 202$ emu mol^{-1} (Fig. 5a), which amounts to a

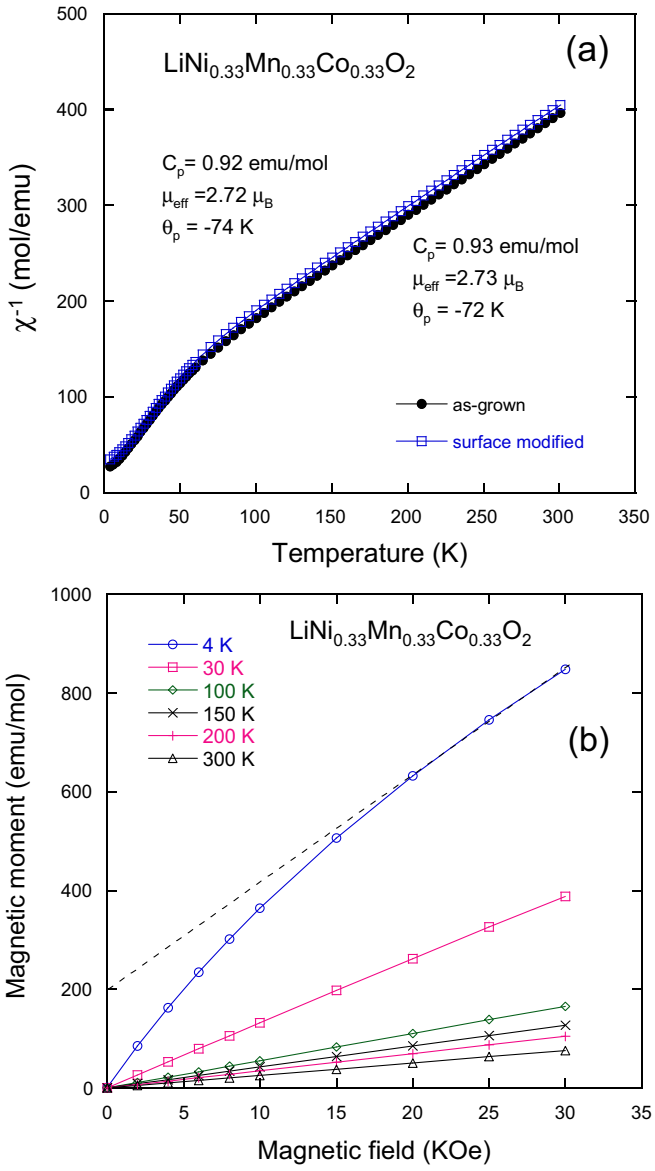

Fig. 5. (a) Plot of the reciprocal magnetic susceptibility H/M for the as-grown and heat-heated samples and (b) isothermal plots of the magnetization $M(H)$ for the as-grown sample. M_s is the magnetic moment at saturation. Note that any difference was observed for the sample heat-treated with sucrose of starch.

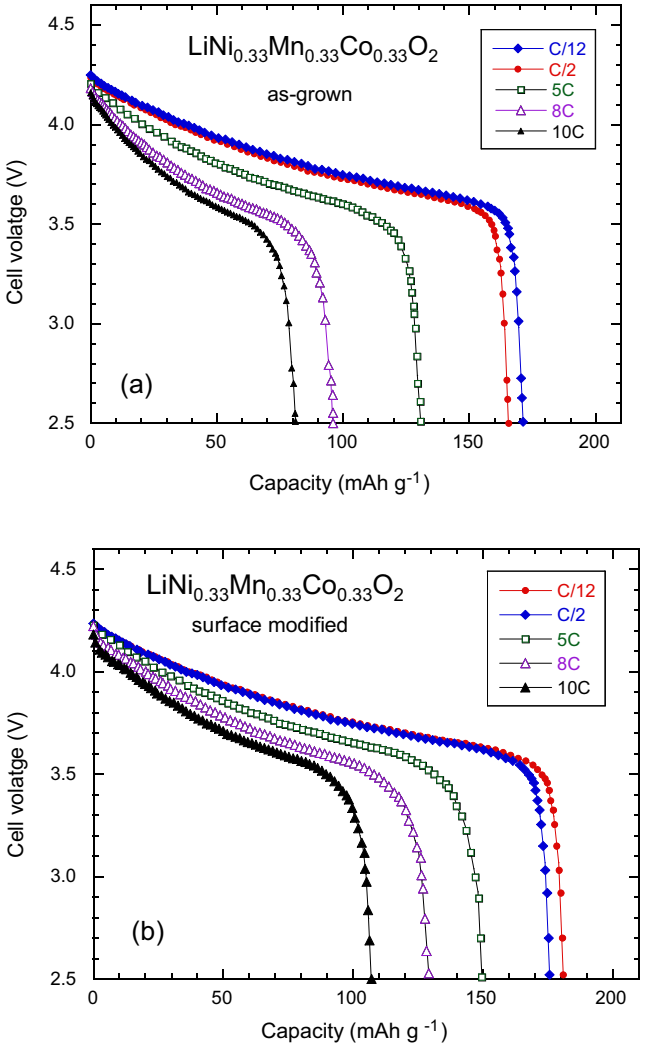

Fig. 6. Discharge cell voltage vs. gravimetric capacity of the Li//LNMCO cells for various C-rate for (a) the as-grown cathode material and (b) the surface modified LNMCO. The electrolyte was 1.0 mol L^{-1} $LiPF_6$ in a mixture of ethylene carbonate (EC) and diethyl carbonate (DEC) (1:1, v/v).

magnetic moment per formula 0.036 μ_B. So the concentration of Ni^{2+} at 3*b* sites can be calculated as 0.036 μ_B/1.67 μ_B = 2.15%, which also agrees well with the results obtained from Rietveld refinement.

3.4. Electrochemical studies

Fig. 6a and b shows the potential vs. gravimetric capacity curves for the second discharge of as-grown and heat treated $LiNi_{1/3}Mn_{1/3}Co_{1/3}O_2$ positive electrode respectively. The cell was cycled between 2.5 and 4.2 V at different C-rates. As shown from the figures both samples display the typical smooth shape of the discharge curves without any plateaus. This indicates that no phase transition occurs during the charge–discharge processes. At C/12, the capacity retention is 171 mAh g^{-1}, which increases to 180 mAh g^{-1} for the surface-modified sample.

Heat-treated samples show not only improvement in the discharge capacity values, but also improvement in the capacity retention upon increasing the C-rate value. By using the same C-rate (C/2) the initial capacity of the surface-modified LNMCO is about 96.8% against 93.2% for the non-treated sample. Therefore, the presence of the disordered surface layer plays an important role on the capacity retention and affects the ratio between the current discharge capacity and the initial capacity vs. cycle number. The same observation can be made at other C-rates values (5C or 8C). With increasing C-rate from 0.5 to 8C the capacity fading recognized for the surface-modified electrode is almost higher than 10% with respect to that of the as-grown cathode material.

The capacity retention of the surface-modified sample at 8C is about 61% from the value obtained at C/2, while this ratio is about 58% for the as-grown sample at the same C-rates. There is also a reduction in polarization in the discharge curve of the surface-modified sample in comparison with that of non-treated sample. This improvement in the electrochemical features is mainly due to the absence of the disordered layer at the surface of $LiNi_{1/3}Mn_{1/3}Co_{1/3}O_2$ particles. This film hinders the fast motion of Li + -ion at the electrode–electrolyte interface and thus reduces the electrochemical performance of the positive electrode.

Fig. 7 shows the Ragone plots for the Li//$LiNi_{1/3}Co_{1/3}Mn_{1/3}O_2$ cells with as-grown and surface-modified cathode material. A

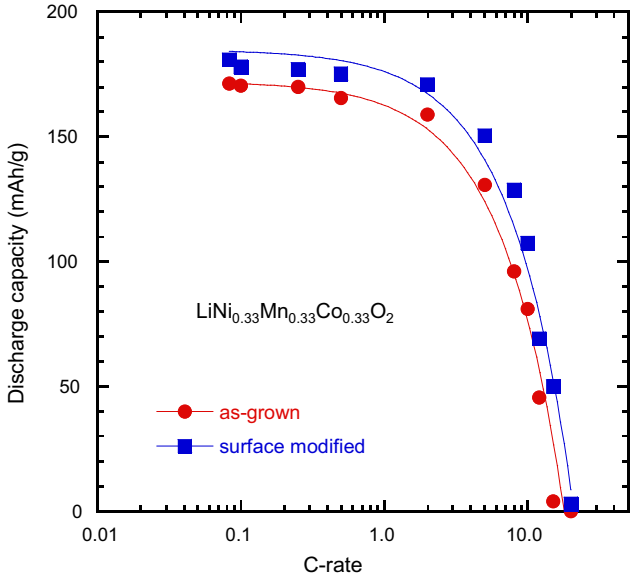

Fig. 7. The Ragone plots of Li cells for the as-grown and the surface modified LNMCO cathode material.

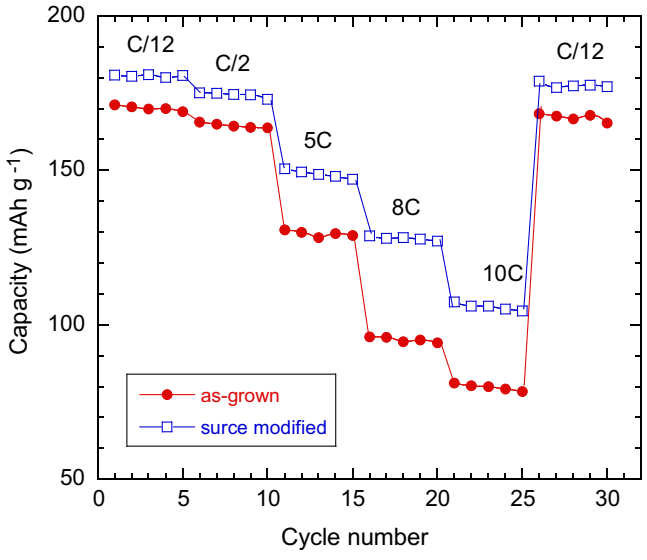

Fig. 8. Discharge capacity between 4.5 and 2.5 V vs. Li^+/Li^0 at various C-rate as a function of cycle number for the as-grown and the surface modified LNMCO cathode material.

capacity 107 mAh g^{-1} is delivered in the voltage range 2.5–4.2 V at current density 10C from the cell with surface-modified $LiNi_{1/3}Co_{1/3}Mn_{1/3}O_2$, while it is only 81 mAh g^{-1} with the non-treated $LiNi_{1/3}Co_{1/3}Mn_{1/3}O_2$ electrode at the same current density. For rate performance comparison, the discharge capacity at various C-rate as a function of cycle number for the as-grown and the surface modified LNMCO cathode material is presented in Fig. 8. For each sample, the cells were tested five times at each C-rate. From these experiments, it is shown that the capacity is recovered with a better efficiency (99.5%) for the surface modified sample than for the as grown cathode material (98.7%) after 25 cycles. The stability of the surface modified LNMCO sample is evidenced by the recovery of the initial capacity.

4. Conclusion

$LiNi_{1/3}Co_{1/3}Mn_{1/3}O_2$ has been synthesized by the co-precipitation method using oxalic acid. Using the prepared particles as starting material, a surface modified material was obtained by heat treatment at 600 °C with a mixture of carbon source. The particles have been carefully characterized using HRTEM and Raman spectroscopy. From these surface analysis experiments, we found that the carbon is not deposited at the surface of particle. However, this treatment reduced the disorder of the surface layer of the as-grown material. This is beneficial for the electrochemical performance of the $LiNi_{1/3}Co_{1/3}Mn_{1/3}O_2$ positive electrode. A capacity higher than 150 mAh g^{-1} is delivered in the voltage range 2.5–4.2 V vs. Li^0/Li^+ at current density C/12-2C with an increase of 8% for the surface-modified $LiNi_{1/3}Co_{1/3}Mn_{1/3}O_2$ cathode material.

References

[1] T. Nagaura, K. Tozawa, Prog. Batteries Solar Cells 9 (1990) 209.
[2] T. Ohzuku, Y. Makimura, Chem. Lett. (2001) 642.
[3] B. Lin, Z. Wen, J. Han, X. Wu, Solid State Ionics 179 (2008) 1750.
[4] J.N. Reimers, J.R. Dahn, J. Electrochem. Soc. 139 (1992) 2091.
[5] S. Zhang, Electrochim. Acta 52 (2007) 7337.
[6] N. Yabuuchi, T. Ohzuku, J. Power Sources 119–121 (2003) 171.
[7] K.M. Shaju, G.V. Subba Rao, B.V.R. Chowdari, Electrochim. Acta 48 (2002) 145.
[8] I. Belharouak, Y.-K. Sun, J. Liu, K. Amine, J. Power Sources 123 (2003) 247.
[9] Z. Lu, D.D. MacNeil, J.R. Dahn, Electrochem. Solid-State Lett. 4 (2001) A200.
[10] D.D. MacNeil, Z. Lu, J.R. Dahn, J. Electrochem. Soc. 149 (2002) A1332.
[11] M.-H. Lee, Y.-J. Kang, S.-T. Myung, Y.-K. Sun, Electrochim. Acta 50 (2004) 939.
[12] D. Aurbach, K. Gamolsky, B. Markovsky, G. Salitra, Y. Gofer, U. Heider, R. Oesten, M. Schmidt, J. Electrochem. Soc. 147 (2000) 1322.
[13] A.M. Kannan, L. Rabenberg, A. Manthiram, Electrochem. Solid State Lett. 6 (2003) A16.
[14] S. Oh, J.K. Lee, D. Byun, W. Cho, B.W. Cho, J. Power Sources 132 (2004) 249.
[15] H.–J. Kweon, J.J. Park, J.W. Seo, G.B. Kim, B.H. Jung, H.S. Lim, J. Power Sources 126 (2004) 156.
[16] K.Y. Chung, W.-S. Yoon, H.S. Lee, J. McBreen, X.-Q. Yang, S.H. Oh, W.H. Ryu, J.L. Lee, W.L. Cho, B.W. Cho, J. Power Sources 163 (2006) 185.
[17] H. Wang, W.-D. Zhang, L.-Y. Zhu, M.-C. Chen, Solid State Ionics 178 (2007) 131.
[18] G. Li, Z. Yang, W. Yang, J. Power Sources 183 (2008) 741.
[19] T.-F. Yi, J. Shu, C.-B. Yue, X.-D. Zhu, A.-N. Zhou, Y.-R. Zhu, R.-S. Zhu, Mater. Res. Bull. 45 (2010) 456.
[20] Z. Chen, J.R. Dahn, Electrochem. Solid-State Lett. 5 (2002) A213.
[21] H.-S. Kim, Y. Kim, S.-I. Kim, S.W. Martin, J. Power Sources 161 (2006) 623.
[22] Y. Kim, H.-S. Kim, S.W. Martin, Electrochim. Acta 52 (2006) 1316.
[23] H.S. Kim, M. Kong, K. Kim, I.J. Kim, H.B. Gu, J. Power Sources 171 (2007) 917.
[24] Q. Cao, H.P. Zhang, G.J. Wang, Q. Xia, Y.P. Wu, H.Q. Wu, Electrochem. Commun. 9 (2007) 1228.
[25] C.M. Julien, A. Ait-Salah, A. Mauger, F. Gendron, Ionics 12 (2006) 21.
[26] X.-Y. Zhang, W.-J. Jiang, A. Mauger, F. Qilu, C.M. Gendron, Julien, J. Power Sources 195 (2010) 1292.
[27] J.R. Dahn, U. von Sacken, C.A. Michal, Solid State Ionics 44 (1990) 87.
[28] T. Ohzuku, A. Ueda, M. Nagayama, J. Electrochem. Soc. 140 (1993) 1862.
[29] A. Abdel-Ghany, K. Zaghib, F. Gendron, A. Mauger, C.M. Julien, Electrochim. Acta 52 (2007) 4092.
[30] P.Y. Liao, J.G. Duh, S.R. Sheen, J. Electrochem. Soc. 152 (2005) A1695.
[31] C. Julien, Solid State Ionics 136 (2000) 887.
[32] D.S. Knight, W.B. White, J. Mater. Res. 4 (1989) 385.
[33] M. Nakamizo, K. Tamai, Carbon 22 (1984) 197.
[34] Y. Hu, M.M. Doeff, R. Kostecki, R. Finones, J. Electrochem. Soc. 151 (2004) A1279.
[35] N. Ravet, M. Gauthier, K. Zaghib, A. Mauger, J. Goodenough, F. Gendron, C.M. Julien, Chem. Mater. 19 (2007) 2595.
[36] M.L. Trudeau, D. Laul, R. Veillette, A.M. Serventi, K. Zaghib, A. Mauger, C.M. Julien, J. Power Sources 196 (18) (2011) 7383–7394.
[37] X. Zhang, C.M. Julien, A. Mauger, F. Gendron, Solid State Ionics 188 (2011) 14.
[38] A. Abdel-Ghany, A. Mauger, F. Gendron, K. Zaghib, C.M. Julien, ECS Trans. 3 (2007) 137.